



Fully Automated Measurement Setup for Photovoltaic Panel Performance Evaluation and Testing under LabVIEW Platform

Mustafa Q. Ali^{1,*}, Monaf S. Tapou¹, Hayder A. Dhahad²

¹ University of Technology, Control and system Engineering Department, Baghdad, Iraq

² University of Technology, Mechanical Engineering Department, Baghdad, Iraq

ARTICLE INFO

ABSTRACT

Article history:

Received 8 January 2020

Received in revised form 19 May 2020

Accepted 20 May 2020

Available online 5 November 2020

Photovoltaic (PV) devices are widely used renewable energy resources and have been increasingly manufactured by many firms and trademarks. This condition makes the selection of right product difficult and requires the development of a fast, accurate and easy setup that can be implemented to test available samples and select the cost effective, efficient, and reliable product for implementation. An automated test setup for PV panels using LabVIEW and several microcontroller-based embedded systems were designed, tested, and implemented. This PV testing system was fully automated, where the only human intervention required was the instalment of PV panel and set up of required testing conditions. The designed and implemented system was characterized by high performance standard with accuracy, precision, and resolution that is good enough to practically test any PV panel of the 12 V and 24 V ratings. In this paper, several simulations run and manually performed testing for PV panels were done to verify the automatically obtained results and those were found to be of good conformity (-3% difference with simulation results, 0.01% with manually taken results).

Keywords:

Photovoltaic; LabVIEW; microcontroller; embedded device; phase control; pulse width modulation

1. Introduction

Solar energy is the most important renewable and sustainable energy source given its availability around the world [1]. Two types of solar energy conversion systems are common, indirect and direct energy conversion systems. Direct energy conversion is realized by converting light energy into electricity through the PV effect. The PV effect is the creation of voltage and electrical current in a material upon exposure to light and is a phenomenon that relies on physical and chemical effects [2]. This work focuses on testing and evaluating the direct energy conversion devices namely the photovoltaic (PV) panels. The prime element of a PV-based power generation plant can be selected from numerous PV panel manufacturers. Accordingly, testing and evaluating PV panels is a vital issue

* Corresponding author.

E-mail address: mustafaqussay@cois.uobaghdad.edu.iq

as it will influence the prudence of the decision made on selecting these prime elements as it will impact the performance and endurance of the to be erected power plant. Additionally, studies focusing on increasing the efficiency of PV devices should be conducted in a simulated environment that can mimic the environmental conditions of the places where they will be deployed. The test requires the use of solar simulators. The light source selection for solar simulators is one of the key points in the testing and evaluation of PV products [3]. Testing PV panel also assists in determining the maximum power point (MPP) of this device which is the maximum power achievable from it for a given irradiance. This point is located through a process termed maximum power point tracking (MPPT) which is done by varying the load applied to the PV panel while measuring the power delivered to the load and then MPP is located which will be applied in the MPP tracking process. Manual testing consumes a very long time with error prone procedures. Automating this process will result in shorter test time and yield more dependable results with automated logging.

This paper presents the design and implementation of a completely automated controlled environment system based on embedded applications intended to test, evaluate, and calculate the MPP for any PV panel operating at any given working condition. This process is initiated by applying different amounts of solar irradiance and temperature that simulate the variation of weather around the year for a given geographical location. A graphic user interface (GUI) is designed using LabView platform to setup the desired parameters that can test the daily performance of a PV panel from dawn to dusk in a year.

2. Previous Works

A lot of work has been done on the subject of evaluating and testing PV panels. The following are those found to be of considerable significance to the subject of the work described in this paper.

Motbahhir *et al.*, [5] presented a designed system for PV panel testing and evaluation using halogen lamps for solar simulation and a rheostat for load. Arduino Uno-based voltage and current measurement system was developed using a solid-state current sensing device. A simulation was conducted on Proteus environment. On evaluating this work, no logging functions were provided, the light source power was not declared to verify its capability in providing the necessary light intensity required for testing. Cuce *et al.*, [6] introduced a controlled room with a solar simulator consisting of twelve 1 KW tungsten halogen bulbs placed in a hood mounted on the top of the test room. Manual control was provided to manage light intensity. Air conditioning system was provided in the experiments under desired ambient temperature. A digital ammeter, voltmeter and pyranometer were used to carry out the required measurements. A rheostat was used as a variable load. Only one solar cell was tested. Lalaoui *et al.*, [7] presented experimental analysis for different kinds of PV panels. Indoor evaluation was performed using state-of-the-art equipment to measure and log the test results. However, this test setup used expensive devices that are not attainable for all researchers. Zaoui *et al.*, [8] developed an experimental setup to evaluate the electrical performance of silicon PV modules using digital multimeters for describing the I–V characteristics, rheostat as a variable load, and a thermometer. A flux meter was used to set the intensity of the halogen light source. However, the test results were manually obtained thereby resulting in logging errors and unnecessary long testing time. Kumar *et al.*, [9] described an experimental setup to obtain the characteristics of a PV cell using a ready-built solar simulator, digital thermometer and digital multimeters for measuring short circuit current and open circuit voltage. A rheostat was used as a variable load. Reviewing this work showed that datalogging and testing were manually performed, making it prone to logging and human errors.

3. PV Panel Testing System Hardware

The fully automated PV test system controls three main parameters that directly affect PV panel performance. These parameters are solar irradiance, ambient temperature and applied load on PV panel. Normally 24 V with up to 300 W rated PV panels are the most common devices in the market, these have an output voltage that could reach about 37 V at low / no load conditions, and a current output that could reach 12.5 A. these figures were considered when selecting the maximum voltage and current rating of the measuring section of the designed testing system. For the voltage the 40 Volts limit was selected giving a measuring overhead of more than 9.25 % while the current measuring system was designed with a 15 A load current limit which was selected to suit the currently available output ratings with addition measuring overhead of 20%. Figure 1 shows the simplified block diagram of the designed PV panel testing system and Figure 2 shows the implemented PV panel test system.

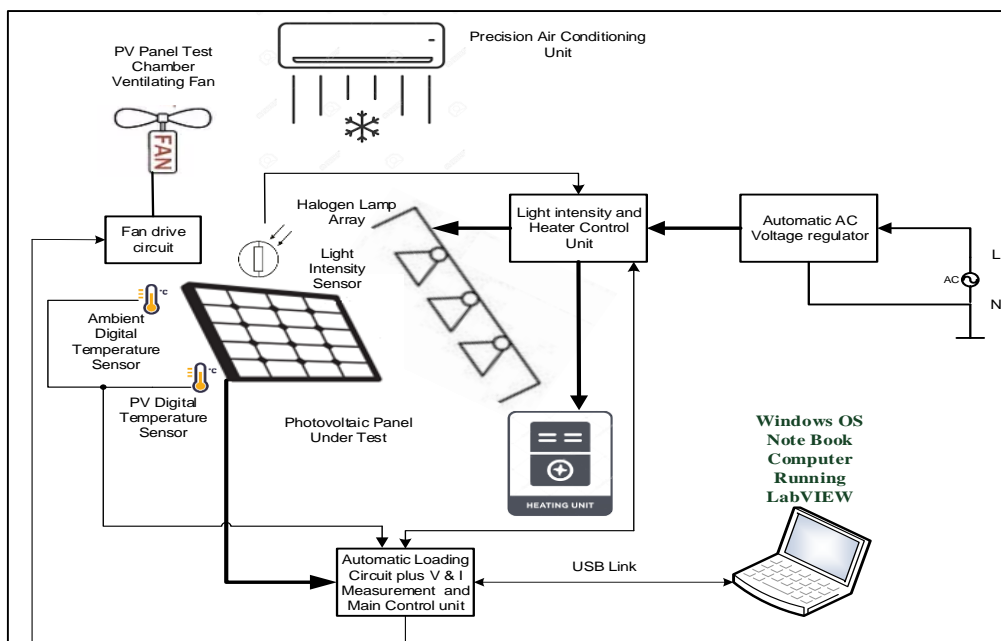


Fig. 1. Block diagram for PV panel testing system

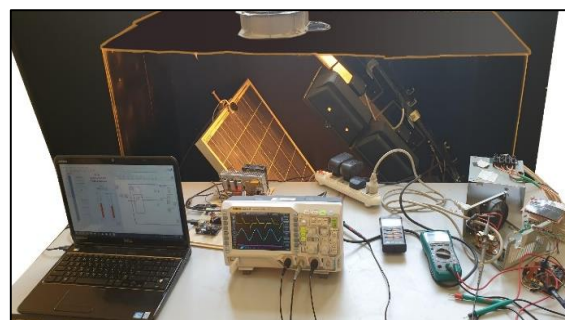


Fig. 2. Fully automated PV testing system

This system is composed of the following units.

3.1 Automated PV Panel Loading Unit

The automated load circuit provides variable load to the PV panel as governed by the test scheme without manual intervention, enabling the load current variation from 0 to $I_{out\ Max}$ for each panel under test. As shown in Figure 3, the circuit is controlled using a 32bit microcontroller (STM32F103X8) that is based on ARM architecture. It generates a 12-bit digital output represented on port A (A0–A11) connected to the 12-bit digital to analogue converter (AD7531) the output of which governs the instantaneous value of PV panel loading. To ensure the operational stability of DAC output, a high-precision voltage reference is implemented using voltage reference IC1 (LM336) for providing a precise and temperature-stable voltage output of 2.5 V. This output is connected to a noninverting operational amplifier (OP90) with a gain equals two to create the required 5 V stable reference to the DAC. The DAC current output is converted to voltage using an inverting current to voltage converter circuit based on OP90. Another OP90 is used to invert the output voltage and provide a gain equalling two. The output voltage of this stage drives the active variable load circuit that is based on the power bipolar transistor ‘BJT’ (BU931P).

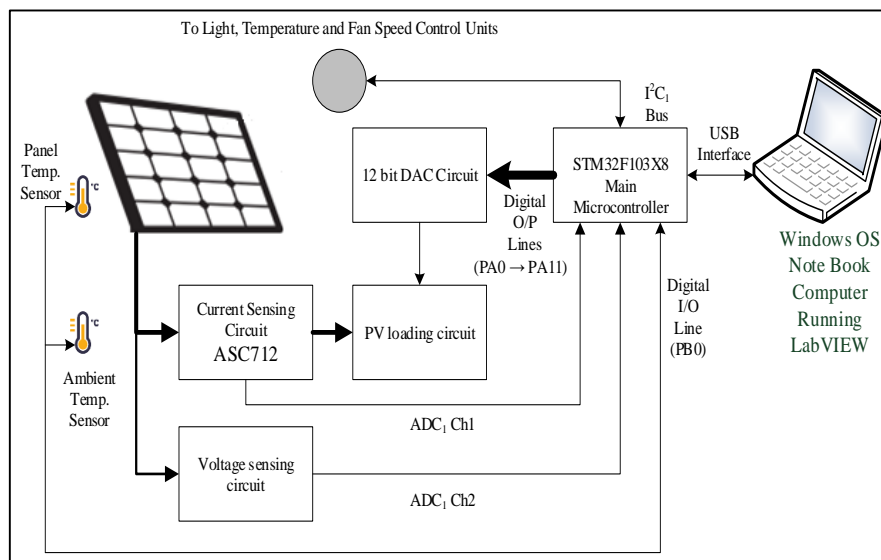


Fig. 3. Block diagram of the automated PV panel loading unit

The active load circuit operates as follows: D1 and D2 thermally compensate the variation of transistor collector saturation current (I_{CO}) of the power BJT. Therefore, reverse saturation current I_O of the diode will increase with temperature at the same rate as I_{CO} .

$$I = \frac{V_{CC} - V_{BE}}{R} \cong \frac{V_{CC}}{R} = Constant \quad (1)$$

The diodes are reverse biased by V_{BB} , and the current through them is the reverse saturation current I_O . The base current is expressed as:

$$I_B = I_D - I_O \quad (2)$$

Substituting the above value in the expression for collector current yields,

$$I_C = \beta(I_D - I_O) + (1 + \beta)I_{CO} \quad (3)$$

If $\beta \gg 1$, then

$$I_C = \beta I_D - \beta I_O + \beta I_{CO} \quad (4)$$

I_D is approximately constant, and I_C remains constant when I_O of diode and I_{CO} of transistor track each other at the operating temperature range. Resistor R11 (0.68 Ω /50 W) is placed between the emitter and ground to provide negative feedback for stable operation and to protect from short circuit condition along with R12 (0.1 Ω /10 W) in case of transistor failure or being driven to saturation. Transistor Q2 operates as an emitter follower that provides the necessary drive current to Q1. Microcontroller MC₁ performs additional functions. It reads the instantaneous PV panel voltage in the range of 0 V to 40 V as well as current in the range of 0 A to 15 A and sends them to the PC via USB. The voltage is fed to ADC₁ pin8 through the voltage sensing circuit that comprises of a voltage sampling divider network and a voltage follower. The divider is set to provide 11.43:1 division factor to suit the ADC maximum input of 3.5 V. The current sensing circuit is designed around ASC712 current sensing device that has a range of 0 A to 30 A with an output of 66 mV/A. Maximum measurement sensitivity requires a noninverting op-amp based amplifier with a voltage gain of 3.54 adjustable to 10%. Noise immunity on ADC inputs is provided using passive low pass filters. The ADC inside the controller provides 12-bit resolution that results in measurement accuracy around 9 mV with ± 4.5 mV error for the voltage measuring function and accuracy of 3.67 mA resolution with ± 1.84 mA error for the current measuring function. These accuracy and error figures were verified against those obtained using Hameg HM 8012 and were found to be conforming with the expected measuring outcome of the automated system. The microcontroller reads the ambient and PV panel temperature using two DS18B20 digital temperature sensors that are connected to microcontroller digital I/O pin PB0. These sensors are provided with a one-wire serial communication interface with each sensor having a unique physical address.

The implemented ventilation fan has built in drive enable and speed control. This fan is operated after applying the test condition to provide homogeneous temperature throughout the test chamber. The drive enable is connected to microcontroller digital I/O pin PB5. The schematic of automated PV loading and measuring circuit is shown in Figure 4.

The flowchart of the program that is used in the PV loading and measuring circuit operation is shown in Figure 5.

3.2 Solar Simulator Intensity and Temperature Control Unit

This unit is composed of two main circuits. The first circuit generates synchronization pulses with mains supply frequency and is a zero-crossing detector that detects the initiation of the sinusoidal waveform of the mains supply. This signal is fed to the controlling device the ATmega 328P microcontroller. This microcontroller along with other circuit elements controls the triggering of two TRIAC devices independently to perform what is termed as *phase control*. This function changes the AC output voltage delivered to load so as to control light intensity of tungsten halogen light source used to simulate solar irradiance, and the heating element thermal output which is used to set ambient temperature to the desired value selected by the required test condition. Figure 6 shows the solar simulator 6 \times 1 KW halogen light used to obtain uniform light distribution and different irradiance values.

An efficient means to control mains AC power delivered to load is by using phase control techniques. Phase control involves the use of TRIACs or thyristors as control devices [10]. In the case of the unit underhand, a TRAC was chosen to govern the amount of AC power delivered to load by changing the effective value of AC voltage on the load (halogen lamp or heater). The switching device is turned on by applying a trigger pulse to its gate terminal after a predetermined delay within each AC half cycle (or cycles) (every 10 mS), in degree terms this corresponds to (0° to 180°) and (180° to 360°) of the sinusoidal cycle. The trigger angle (α) is the delay of the trigger pulse delivered to the gate terminal within each AC half cycle. Figure 7 shows the AC mains supply waveform along with the trigger pulse and the resulting load voltage waveform.

The solar simulator circuit receives its set point from the active load control system which in turn receives this value from the one set by user on the desktop of the control and monitoring computer running a specially developed application running under LabVIEW platform [11]. Figure 8 shows the desktop of the user interface of the LabVIEW based testing software.

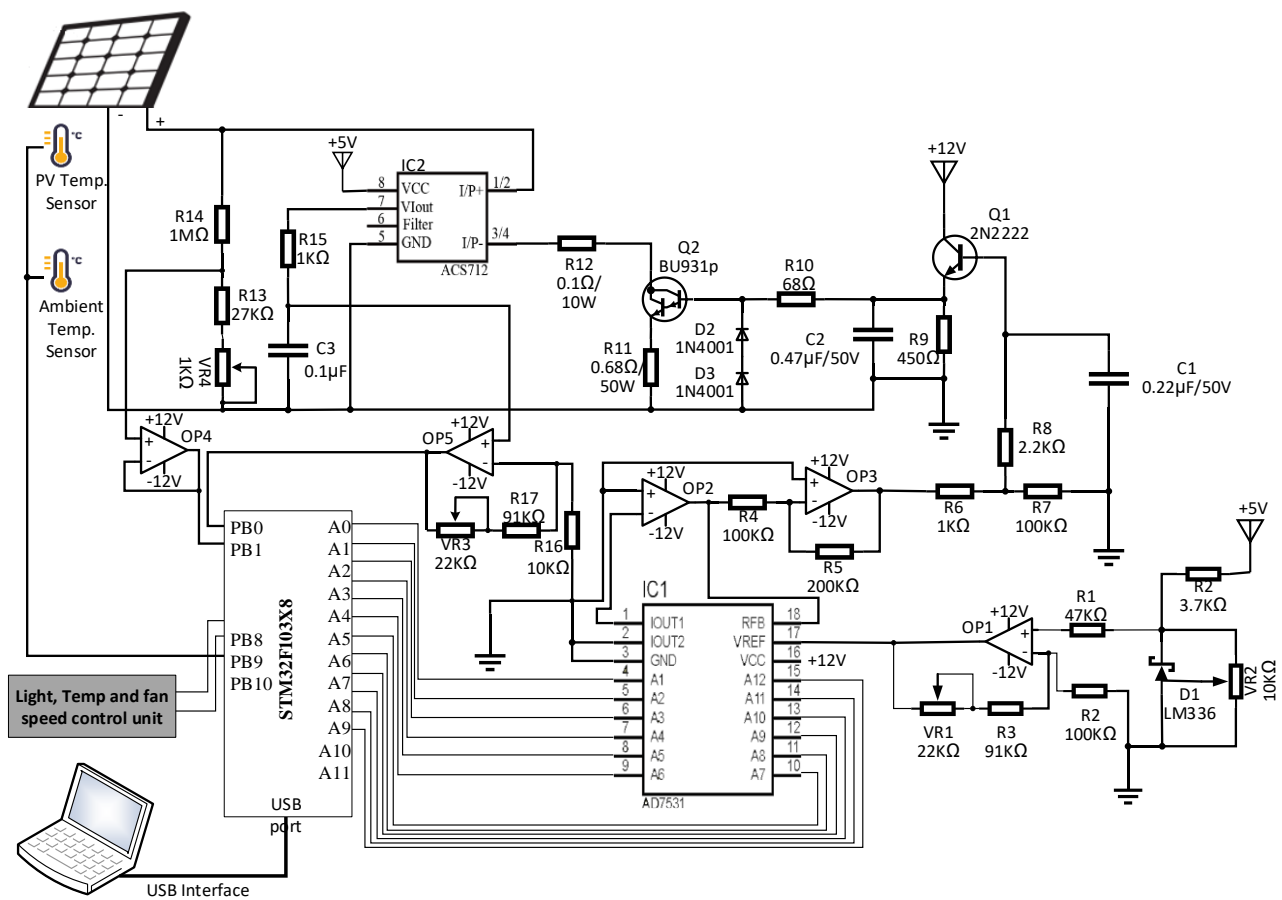


Fig. 4. Automated load circuit schematic

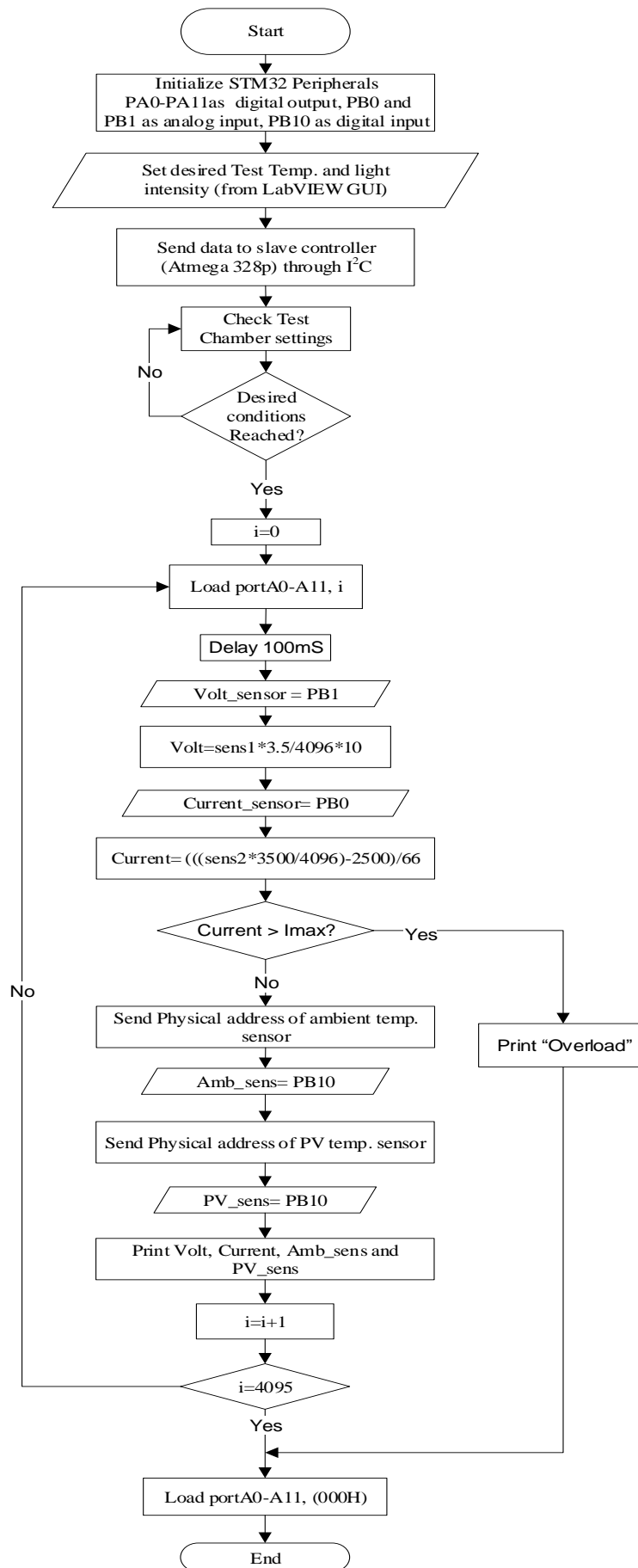
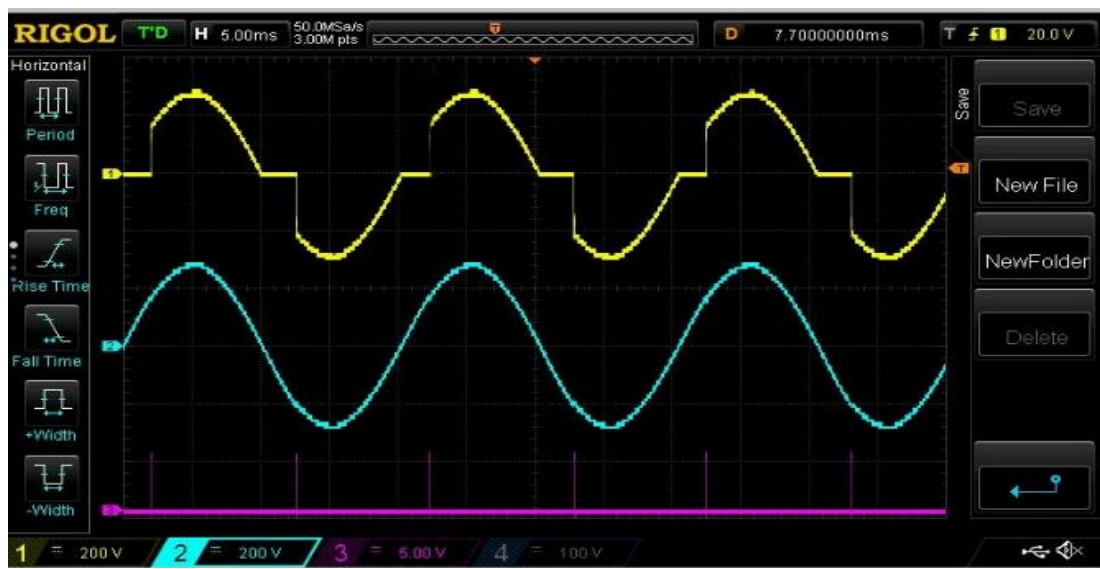


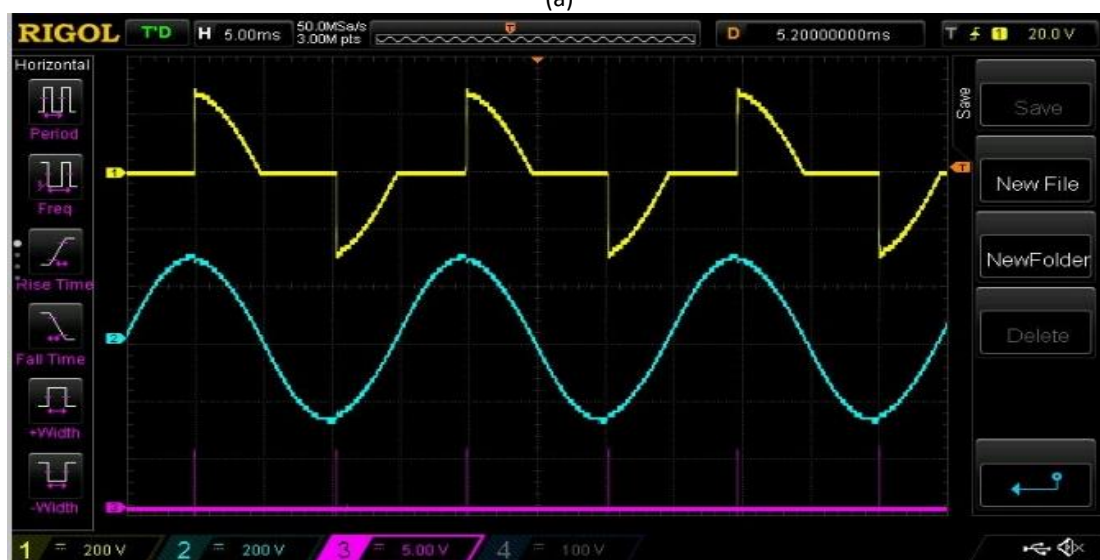
Fig. 5. Flowchart of program



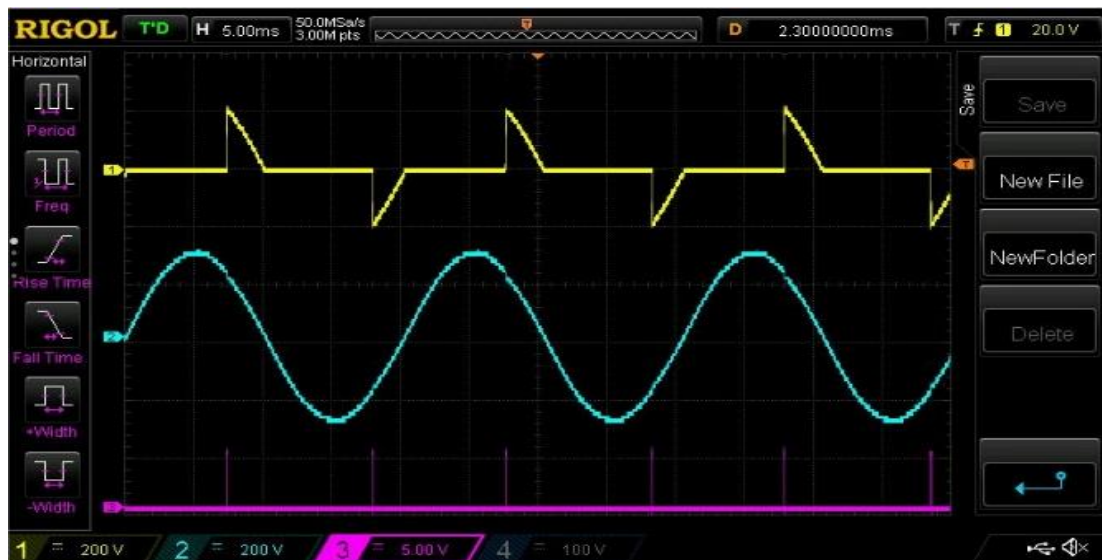
Fig. 6. Lights and PV panel



(a)



(b)



(c)

Fig. 7. Input(blue), trigger (purple) and output (yellow) waveforms of phase control a) when $\alpha=25\%$, b) when $\alpha=50\%$, and c) when $\alpha=75\%$

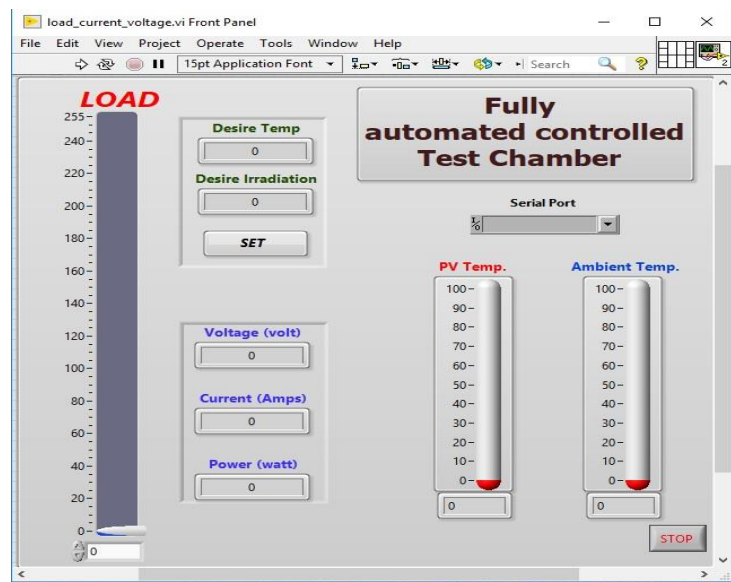


Fig. 8. Graphical user interface under LabView platform

The control action is of closed-loop type, and an optical sensor monitors generated the light intensity feedback, where its output is calibrated in W/m^2 . The light intensity sensor uses a light dependent resistor (LDR) as a light intensity detector. The value of radiation required to implement the test starts from $0 W/m^2$ up to $1000 W/m^2$. Light radiation incident to light detecting element attenuated to a specific amount prevent saturating the detector. A simple means is to use two optical polarizer sheets that are rotated at $\pm 45^\circ$ angle between each other. Figure 9 shows the response of the light sensing circuit after shading.

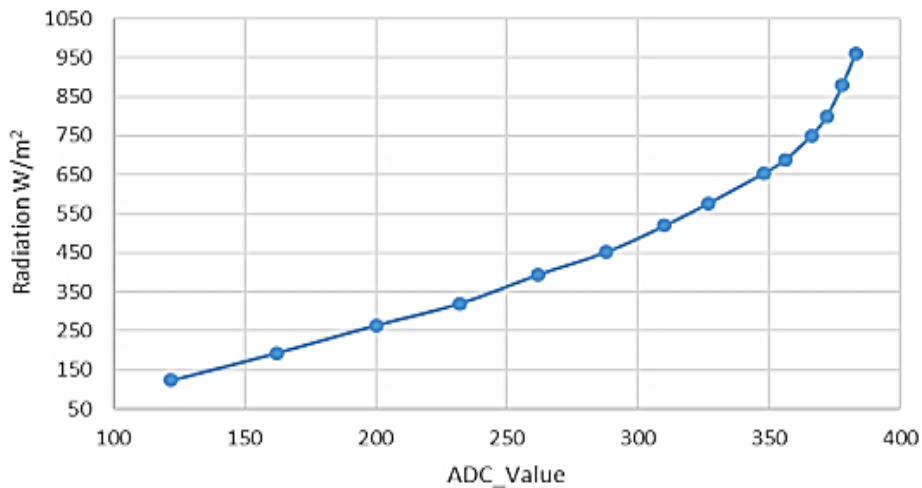


Fig. 9. LDR response after the shading

The heating unit is monitored by the digital thermometer (DS18B20), this sensor readings are delivered through one wire serial communication scheme. It is connected to the digital I/O pin (PD7) of the micro controller. The controller changes trigger angle (α) so as to change by the amount of electrical power delivered to halogen lamps in order for them to generate the desired light intensity, or to the heating element to change the amount of heat generated to rise ambient temperature to the desired degree Celsius. The counter/timer 1 module in the microcontroller was used to generate the trigger pulses as it has two independent outputs that can be separately controlled by loading the proper value into the specific special function registers (OCR1A, OCR1B).

A fuzzy logic control (FLC) scheme was developed to optimize the response of the light intensity and temperature control operations. The Mamdani model is implemented as being a well proven method to build an FLC [12].

The light intensity control is adopted to the structure of two inputs and one output fuzzy set. The first input named V_{in} is defined as the input voltage need to obtain the set value of light intensity with values range between 0 V to 220 V. The second input named light is define as the feedback value of light intensity sensor with values ranges from 0 W/m² to 1000 W/m². The output (α) represents the value of trigger angle with values range from 0° to 180° to satisfy the amount of electrical power that reaches the load. These fuzzy sets had five triangular membership functions, as shown in Figure 10.

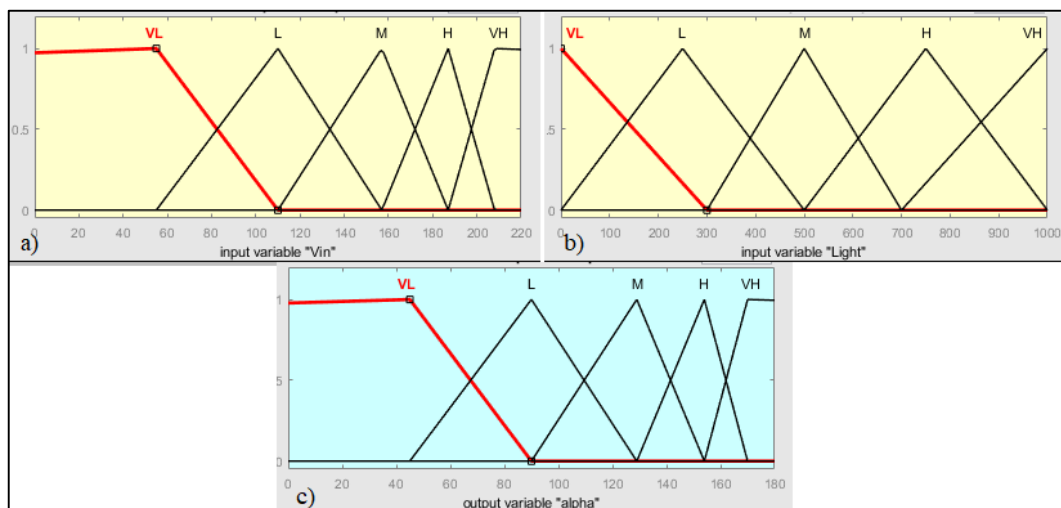


Fig. 10. Fuzzy sets of light intensity FLC

Table 1 shows the fuzzy rule sets used to implement light intensity FLC.

Table1

Fuzzy rule sets of light intensity FLC

Vin Light	VL	L	M	H	VH		
VL	VL	VL	VL	L	M	VL	Very low
L	VL	VL	L	M	H	L	Low
M	VL	L	M	H	VH	M	Medium
H	L	M	H	VH	VH	H	High
VH	M	H	VH	VH	VH	VH	Very High

The temperature FLC also adopted with two inputs and one output fuzzy set. The first input named error represents the desire temperature set point minus the feedback value of the sensor with range between -50°C to 50°C. The second input variable is a change in error (derror) derived from the difference of the last error and instant error [13]. The trigger angle (α) represents the output variable for temperature of FLC, its value ranges from 0° to 180° to satisfy the amount of electrical power that reaches to the load. Figure 11 shows the fuzzy sets with seven triangular membership function provide the desired improvement in system response.

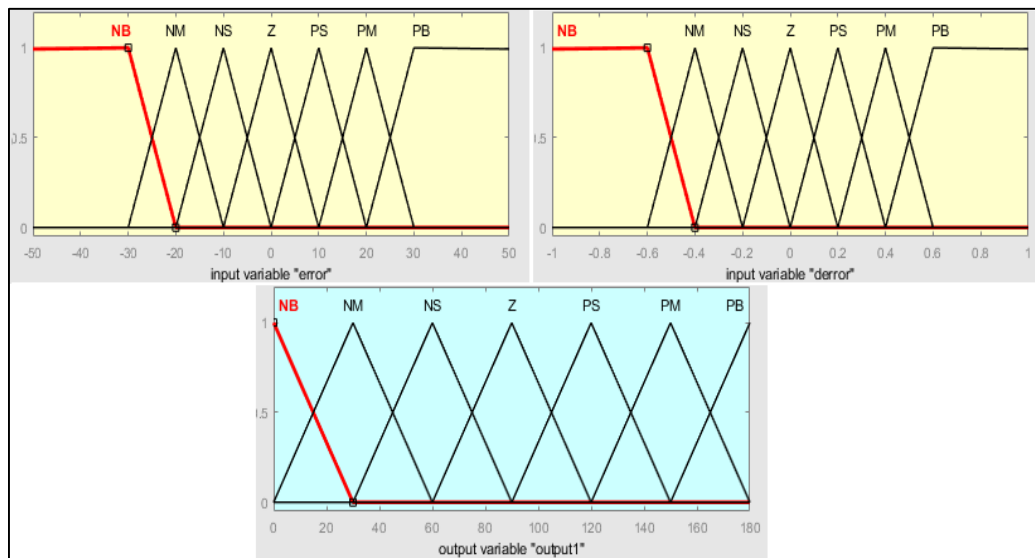


Fig. 11. Fuzzy sets of temperature FLC

Table 2 shows the control base rules for the implemented temperature FLC.

Table 2

Fuzzy rule sets of temperature FLC

error derror	NB	NM	NS	Z	PS	PM	PB		
NB	NB	NB	NM	NM	NS	NS	Z	NB	negative big
NM	NB	NM	NM	NS	NS	Z	PS	NM	negative medium
NS	NM	NM	NS	NS	Z	PS	PS	NS	negative small
Z	NM	NS	NS	Z	PS	PS	PM	Z	zero
PS	NS	NS	Z	PS	PS	PM	PM	PS	positive small
PM	NS	Z	PS	PS	PM	PM	PB	PM	positive medium
PB	Z	PS	PS	PM	PM	PB	PB	PB	positive big

To successfully implement phase-control technique for the voltage controller, the controller needs the value of the angle with respect to the zero crossing (the moment when the voltage crosses zero value) of the sinusoidal AC power waveform to synchronize the controlling timer (timing the value of angle α) with respect to main AC voltage. The synchronizing signal generated by the electronic circuit is shown in Figure 12.

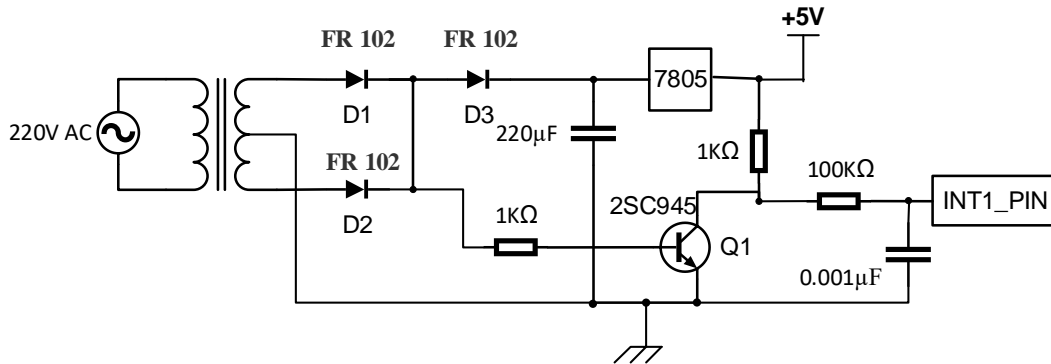


Fig. 12. Synchronization signal circuit

Diodes D1 and D2 represent a full wave rectifier for center tap transformer. Thus, Q1 will turn off when the voltage is less than 0.6 V (minimum) and will turn on when the voltage passes 0.6 V. In this way, pulses will be generated and synchronized with the zero-crossing point. The output is taken after a passive low pass filter to reject high frequency noise associated with the generated signal.

TRIAC (BTA41) is implemented for the light intensity and heater drive circuits. Isolation from the main voltage (220 Vac) is important for operator and computer electronics safety. The MOC 3041 opto-isolator device is selected for this purpose. The additional RC components are snubber circuit that function as switching stress reduction device for load driving TRIACs. The complete diagram of the phase control circuit is shown in Figure 13.

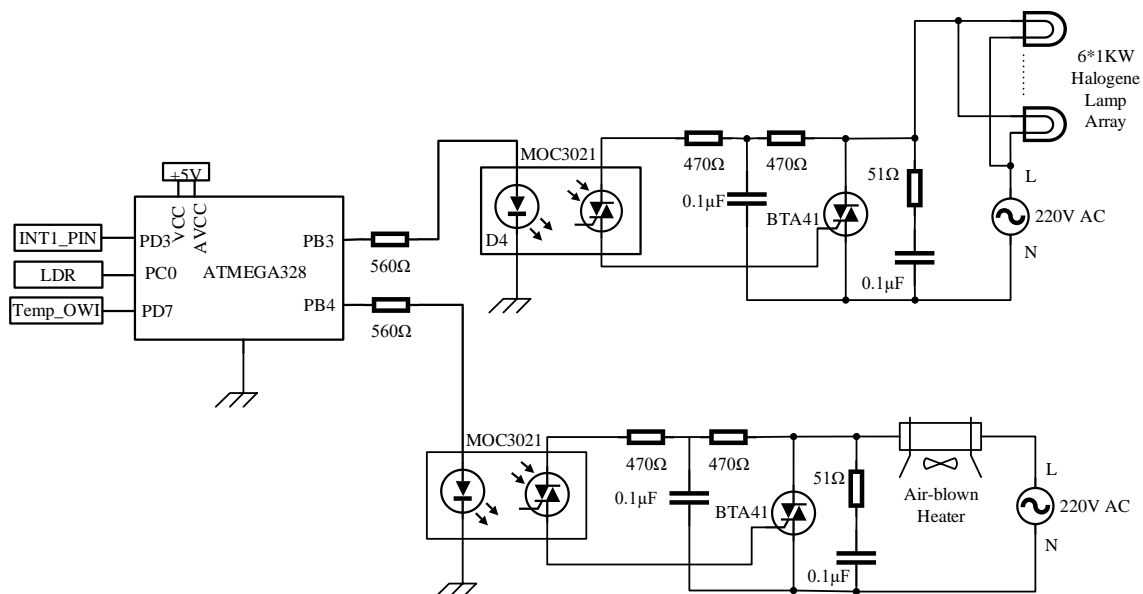


Fig. 13. The complete circuit of light intensity and temperature phase control

4. Mathematical Model

The simple means to characterize a solar cell is by considering a current source connected in parallel with an ideal diode, which can be expressed as

$$I = I_{pv} - I_D \tag{5}$$

Two resistors are added to the circuit to improve expression (5) and to better fit the cell behaviour, as shown in Figure 14. The first resistor is a shunt resistor (R_{sh}) that represents the current leakage through the high resistivity shunts across the p–n junction and is added in parallel with the source and the diode. The second resistor (series resistance, R_s) is connected in series and represents the losses in cell solder bonds, interconnection, and junction box [14].

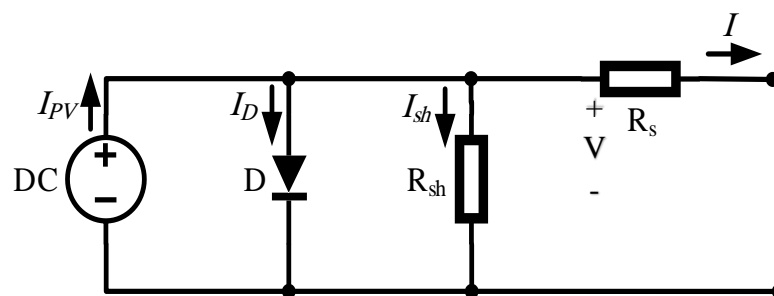


Fig. 14. Improved equivalent circuit of solar cell

With the improved circuit in Figure 14 and applying Kirchhoff's law, the following equivalent equation for the load current is obtained

$$I = I_{pv} - I_D - I_{sh} \tag{6}$$

where I_D is defined by (Shockley diffusion theory) as the ideal recombination current from the diffusion and recombination of electrons and holes in p and n sides of the cell and is written as [14]

$$I_D = I_o \times \left[\exp \left(\frac{V + IR_s}{a V_T} \right) - 1 \right] \tag{7}$$

where I_o is the diode reverse saturation current.

A nondimensional constant a is added to the term of the recombination current in the p- and n-sides. This constant is called the ideality or quality factor (or sometimes emission coefficient) and considers the deviation of the diodes from Shockley diffusion theory (the value of factor a is assumed to be constant, 1.3 for polycrystalline PV cell, and 1.2 for monocrystalline PV cell) [15]. V_T is the thermal voltage expressed as [16]

$$V_T = \frac{N_s k T}{q} \tag{8}$$

where T is the temperature in Kelvin, and k is the Boltzmann constant. q is the charge of the electron, and N_s is the number of series connected cells.

Using Ohm's law, the current occupied in the shunt resistor is expressed as [16]

$$I_{sh} = \frac{V+IR_s}{R_{sh}} \quad (9)$$

The 1-diode/2-resistors circuit model is expressed as [17]

$$I = I_{pv} - I_o \times \left[\exp\left(\frac{V+IR_s}{aV_T}\right) - 1 \right] - \left(\frac{V+IR_s}{R_{sh}}\right) \quad (10)$$

The PV cell photocurrent, which depends on the radiation and the temperature, is given by [17]

$$I_{pv} = [I_{sc} + K_i(T - T_n)] \times \frac{G}{G_n} \quad (11)$$

where I_{sc} is the short circuit current, K_i is the solar cell current temperature coefficient (0.0017), G is the irradiance (W/m^2), and G_n and T_n is the irradiance and temperature at standard term condition (STC). A solar cell has two states, namely, open circuit and short circuit. At open circuit state, the output current is equal to zero, and the voltage is the open circuit voltage. These values are substituted in Eq. (10) to obtain nominal diode reverse saturation current (I_{on}) as [17]

$$I_{on} = \frac{I_{sc}}{\exp\left(\frac{V_{oc}}{aV_T}\right) - 1} \quad (12)$$

Diode reverse saturation current (I_o) is obtained using the following equation [14]

$$I_o = I_{on} \left(\frac{T_n}{T}\right)^3 \exp\left[\left(\frac{qE_g}{aK}\right) * \left(\frac{1}{T_n} - \frac{1}{T}\right)\right] \quad (13)$$

where E_g is the band gap of silicon at 25 °C.

The mathematical model is implemented using MATLAB Simulink. An 80 W/12 V polycrystalline PV panel from Tapan solar energy PVT Inc. with specification given in Table 3 is used to compare the mathematical and experimental results.

Table 3
 Specification of used PV panel

Parameter	Value
manufacturer	Tapan solar energy PVT Inc
Model	TSE-80P
Max. power (MPP)	80.52 W
Voc	21.89 V
Isc	4.98 A
Rs	0.002 Ω
Rsh	100 KΩ
Ns	36
Gn	1000 W/m ²
Tn	25 °C
Ki	0.0017
Q	1.602×10 ⁻¹⁹ coulombs
K	1.381×10 ⁻²³ J/K
α	1.3

The complete block diagram of this model shows in Figure 15.

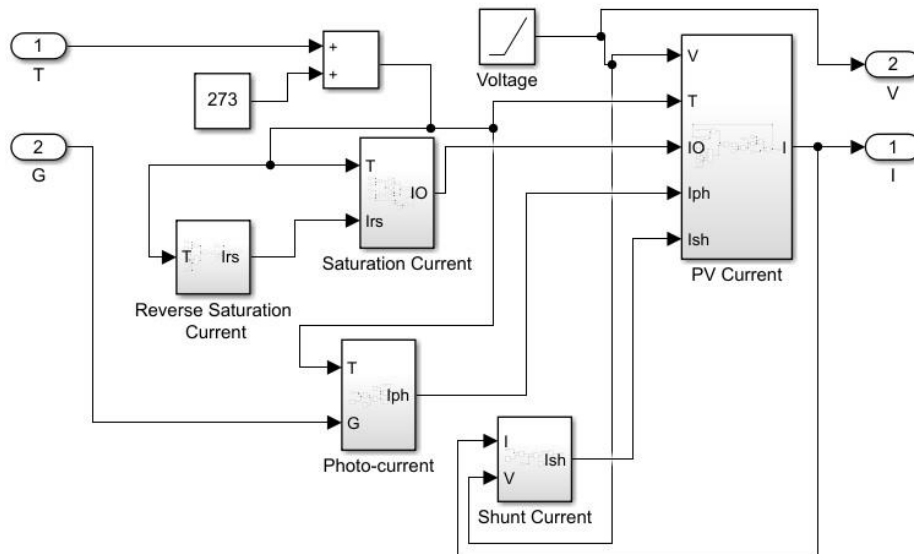


Fig. 15. MATLAB simulink of a PV panel model

5. Results and Discussion

The designed fully automated PV panel tester was put into practice to run several testing cycles on an 80 W/12 V polycrystalline PV panel with manufacturer specifications shown in Table 3 to check the repeatability of measurement results. The obtained results were identical within 0.906 %, proving that this test setup had high precision. The results logged by the computer were compared with the manually obtained results that were taken using the Hameg HM8012 digital multimeter and a 50 Ω /250 W loading rheostat. The obtained results were close within 0.011%, indicating this system has the measurement accuracy that makes it very suitable for the designated purpose. The tested PV panel was subjected to additional repeated test cycles under different irradiances and temperatures inside the test chamber to simulate the effect of solar irradiance variation on PV panel output power throughout one calendar year in order to plot the power–voltage curve and track the MPP of this panel a year around.

The first part of the test showed the effect of solar irradiation on PV panel behaviour under three different irradiances. At 300 W/m², the MPP equal 22.61 W, Voltage at maximum power (V_{mp}) equal 15.5 V and current at maximum power (I_{mp}) equal 1.45 A. When the irradiance is 500 W/m² the MPP equal 39.49 W, V_{mp} equal 16 V and I_{mp} equal 2.39 A. At 800 W/m², the MPP equal 62.25 W, V_{mp} equal 16.5 V and I_{mp} equal 3.77 A. All These results are taken with fixed ambient temperature of 25 °C. As shown in Figure 16, the increasing solar irradiance led to increase the open circuit voltage and the short circuit current and hence the maximum power point increase. However, by increasing the irradiance, PV panel temperature is also increasing, and this adversely affects output power and service life of the PV panel as explained in the next paragraph.

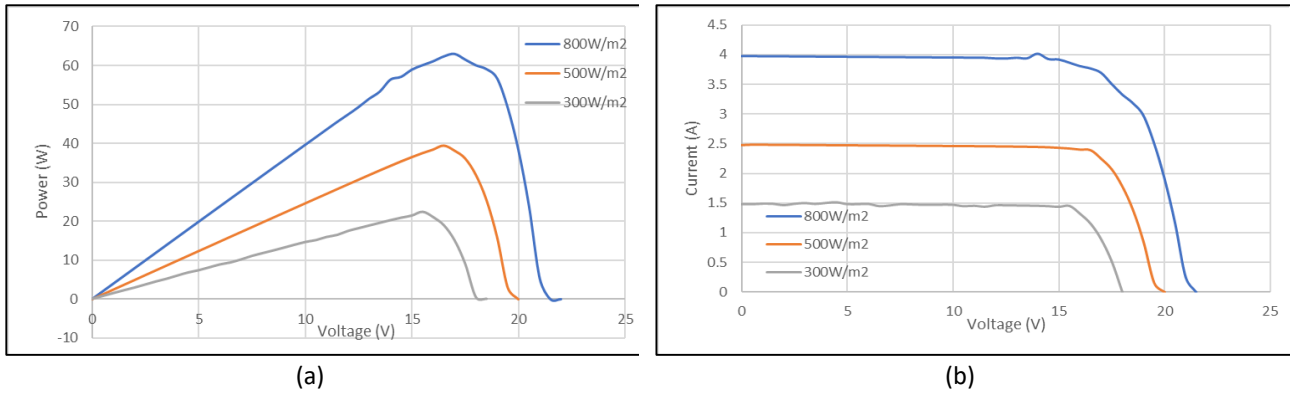


Fig. 16. (a) voltage – power curve and (b) voltage – current curve

The second part of the test shows the effect of temperature variation on PV panel behaviour by taking three different temperature settings (25 °C, 35 °C and 45 °C) with fixed irradiance of 1000 W/m². At 25 °C, the MPP equalled 79.79 W, while V_{mp} equalled 16.5 V and I_{mp} equalled 4.83 A. At 35 °C, the MPP equalled 72.04 W, whereas V_{mp} equalled 15.5 V and I_{mp} equalled 4.847 A. At 45 °C, the MPP dropped to 66 W, however V_{mp} dropped to 13.5 V and I_{mp} to 4.89 A.

In this test, the effect of increased ambient temperature on the output power of PV panel was demonstrated. It has been found that an increase in environment temperature causes a decrease in open circuit voltage and output power, as shown in Figure 17(a). The rise in environment temperature leads to increase in short circuit current but in a marginally smaller proportion which will not contribute to a noteworthy increase PV panel power output, as shown in Figure 17(b).

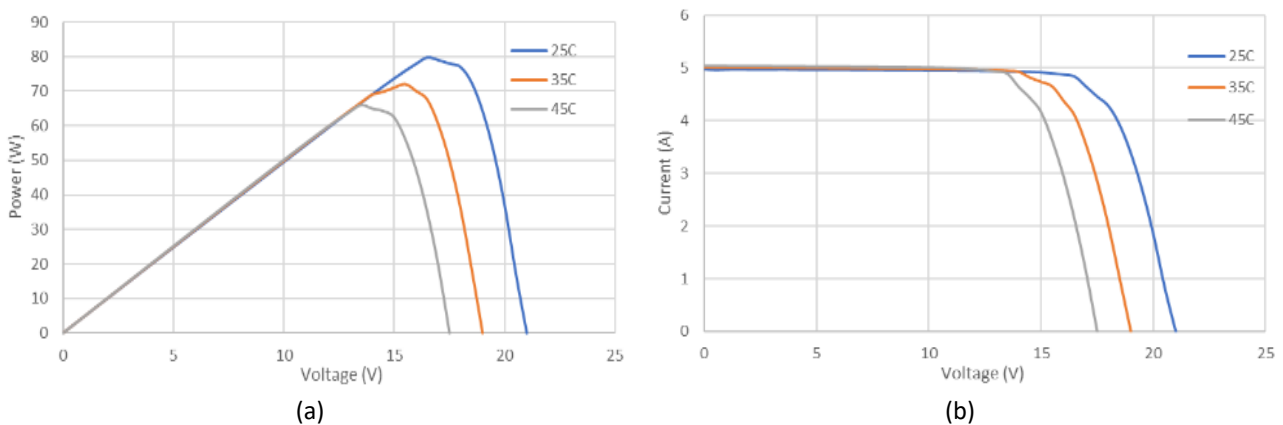


Fig. 17. (a) P-V curve with (b) I-V curve with variation of temperatures

Additionally, a comparison of the experimental and MATLAB simulation results was conducted to validate the functionality and performance of the fully automated controlled test chamber against theoretically obtained results, as shown in Figure 18. Upon verifying, the empirical results had good conformity with MATLAB estimated values and were within –3%. These discrepancies observed between simulation and experimental results can be attributed to not including all possible variables affecting the operation of PV panel in the PV cell model used in the simulation process.

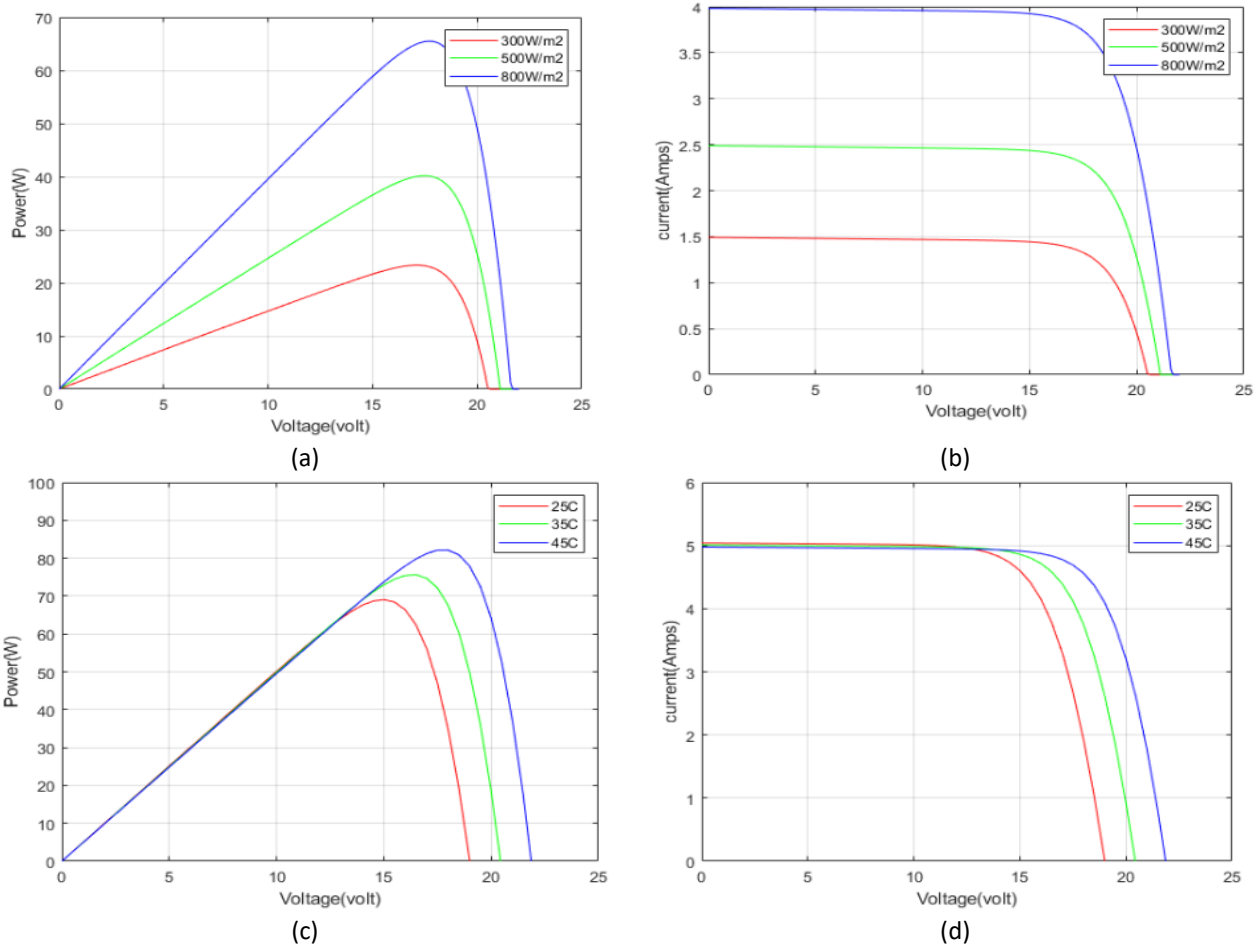


Fig. 18. Simulation result (a) P-V curve with variation of irradiation. (b) I-V curve with variation of irradiation. (c) P-V curve with variation of temp. (d) I-V curve with variation of temp

PV panels from other manufacturers were put under test using the designed testing system and Table 4 shows the discrepancies obtained from simulation results, testing results and manufacturer’s provided parameters. The test results were also verified by performing manual tests on those PV panels and were found to be of high conformity. These test outcomes prove that the results obtained from the designed automatic PV testing system to be highly dependent and accurate and this system can be reliably used to evaluate PV panels.

Table 4

The discrepancies obtained from manufacturer specifications, simulation results, and testing results

PV Panel	Parameters	Manufacturer specifications	Simulation results	Experimental results
Monocrystalline module 300W-72M From Tenka Solar	Pmax	300 W	300.62 W	299.51 W
	Vmp	37 V	37 V	36.75 V
	Imp	8.11 A	8.12 A	8.15 A
Multicrystalline Bp MSX 120 solar panel array	Pmax	120 W	122.7 W	119.52 W
	Vmp	33.7 V	35 V	33.61 V
	Imp	3.56 A	3.50 A	3.55 A
Solarex MSX60 Polycrystalline Photovoltaic module	Pmax	60 W	59.79 W	59.24 W
	Vmp	17.1 V	17 V	16.88 V
	Imp	3.5 A	3.517 A	3.51

6. Conclusions

The implemented automated measurement system is characterized by high performance standard with accuracy, precision, and resolution that the obtained results were identical within 0.906 % with the manufacturer specifications, and within 0.011% comparing with the manual testing. These results are good enough to practically test any PV panel of the 12 V and 24 V rating. In this system, the light intensity can be varied between 0 W/m² and 1000 W/m² and the environmental temperature can be set from 16 °C to 55 °C. So, the output power of the PV panel can be measured at a setting that suits the intended deployment area environment, and it takes within seven minutes to complete PV panel testing and evaluation for one environmental setting. This system is capable of testing commercial PV panels. It has a maximum output voltage range of 40 V with 9 mV resolution and ±4.5 mV error, while the maximum PV panel output current was set to 15 A with 3.67 mA resolution and ±1.84 mA error. The system has the flexibility to change its current range to 30 A. For these reasons, this automated PV test system can assist in conducting researches leading to enhancements in power output of PV panels as required under different installation and operating conditions.

References

- [1] Wang, Guangyu. *Technology, Manufacturing and Grid Connection of Photo-voltaic Solar Cells*. John Wiley & Sons, 2018. <https://doi.org/10.1002/9781119035183>
- [2] Dupré, Olivier. "Physics of the thermal behavior of photovoltaic devices." PhD diss., Lyon, INSA, 2015.
- [3] Esen, Vedat, Şafak Sağlam, and Bülent Oral. "Light sources of solar simulators for photovoltaic devices: A review." *Renewable and Sustainable Energy Reviews* 77 (2017): 1240-1250. <https://doi.org/10.1016/j.rser.2017.03.062>
- [4] Tofoli, Fernando Lessa, Dênis de Castro Pereira, and Wesley Josias de Paula. "Comparative study of maximum power point tracking techniques for photovoltaic systems." *International Journal of Photoenergy* 2015 (2015). <https://doi.org/10.1155/2015/812582>
- [5] Motahhir, Saad, Abdelilah Chalh, Abdelaziz Ghzizal, Souad Sebti, and Aziz Derouich. "Modeling of photovoltaic panel by using proteus." (2017). <https://doi.org/10.25103/jestr.102.02>
- [6] Cuce, Erdem, Tulin Bali, and Suphi Anil Sekucoglu. "Effects of passive cooling on performance of silicon photovoltaic cells." *International Journal of Low-Carbon Technologies* 6, no. 4 (2011): 299-308. <https://doi.org/10.1093/ijlct/ctr018>
- [7] Lalaoui, Lazhar, Mohamed Bouafia, Said Bouzid, Matthias Kugler, Maximilian Zentgraf, Philip Schinköthe, and Sabine Nieland. "Indoor and Outdoor Measurements of PV Module Performance of Different Manufacturing Technologies." In *International Conference on Electrical Engineering and Control Applications*, pp. 238-250. Springer, Cham, 2017. https://doi.org/10.1007/978-3-319-97816-1_18
- [8] Zaoui, F., A. Titaouine, Mohamed Becherif, Mahieddine Emziane, and Abdennacer Aboubou. "A combined experimental and simulation study on the effects of irradiance and temperature on photovoltaic modules." *Energy Procedia* 75 (2015): 373-380. <https://doi.org/10.1016/j.egypro.2015.07.393>
- [9] Prasad, Rahul, Suresh Gawre, and Nikhil Kumar. "Modelling and Simulation of Solar Photovoltaic System and Interfacing with Closed Loop Boost Converter and Neutral Point Clamped Multilevel Inverter." *Electrical and Electronics Engineering: An International Journal* 4, no. 4 (2015): 77-97.
- [10] Rashid, Muhammad H. *Power electronics handbook: devices, circuits and applications*. Elsevier, 2010.
- [11] Ariffin, N. H., and N. Arsadb. "Design of PID Control System Assisted using LabVIEW in Biomedical Application." *Journal of Advanced Research in Applied Mechanics* 15, no. 1 (2015): 1-9.
- [12] Reznik, Leon. *Fuzzy controllers handbook: how to design them, how they work*. Elsevier, 1997.
- [13] Noor, Ilanur Muhaini Mohd, and Muhammad Kamal Mohammed Amin. "Optimized parameters of wastewater treatment system using fuzzy control." *Journal of Advanced Research in Applied Sciences and Engineering Technology* 5, no. 2 (2016): 27-35.
- [14] Rekioua, Djamila, and Ernest Matagne. *Optimization of photovoltaic power systems: modelization, simulation and control*. Springer Science & Business Media, 2012. https://doi.org/10.1007/978-1-4471-2403-0_7

-
- [15] Said, Samer, Ahmed Massoud, Mohieddine Benammar, and Shehab Ahmed. "A Matlab/Simulink-based photovoltaic array model employing SimPowerSystems toolbox." *Journal of Energy and Power Engineering* 6, no. 12 (2012): 1965.
- [16] Hamdi, Roshen Tariq Ahmad. "Solar cell system simulation using Matlab-Simulink." *Kurdistan Journal of Applied Research* 2, no. 1 (2017): 45-51. <https://doi.org/10.24017/science.2017.1.5>
- [17] Belkassmi, Y., A. Rafiki, K. Gueraoui, L. Elmaimouni, O. Tata, and N. Hassanain. "Modeling and simulation of photovoltaic module based on one diode model using Matlab/Simulink." In *2017 International Conference on Engineering & MIS (ICEMIS)*, pp. 1-6. IEEE, 2017. <https://doi.org/10.1109/ICEMIS.2017.8272965>
- [18] Thu, Kyaw, and Yin Maung Maung. "Modelling of a Solar Cell Considering Single-Diode Equivalent Circuit Using Matlab/Simulink." *International Journal of Electronics and Communication Engineering* 6, no. 6 (2019): 5–9. <https://doi.org/10.14445/23488549/IJECE-V6I6P102>